Diamond & Related Materials 139 (2023) 110275

Contents lists available at ScienceDirect

Diamond & Related Materials

journal homepage: www.elsevier.com/locate/diamond

Electrolyte performance of green synthesized carbon quantum dots from fermented tea for high-speed capacitors

Canan Baslak [a], Serkan Demirel [b], Adem Kocyigit [c,*], Mehmet Okan Erdal [d], Murat Yıldırım [e]

[a] Department of Chemistry, Science Faculty, Selcuk University, Konya, Turkey
[b] Vocational High School, Department of Electric and Energy, Igdir University, Igdir, Turkey
[c] Vocational High School, Department of Electronics and Automation, Bilecik Seyh Edebali University, Bilecik, Turkey
[d] Meram Vocational School, Necmettin Erbakan University, Konya, Turkey
[e] Department of Biotechnology, Science Faculty, Selcuk University, Konya, Turkey

ARTICLE INFO

Keywords:
Carbon quantum dots
Fermented tea
Supercapacitor
Electrolyte

ABSTRACT

In recent years, obtaining carbon nanomaterials from natural products by natural methods has been among the most popular topics. The materials synthesized by this way have beneficial properties such as biocompatible, photostable and less harmful for environment. In this study, carbon quantum dots (CQDs) were synthesized by using fermented tea as a natural material and carbon source. The capacitor performance as an electrolyte was investigated with high-speed charge-discharge method as unusual in the literature. The characterizations of the CQDs were realized by HRTEM, XRD, XPS, UV–Vis absorption, and fluorescence spectroscopy techniques. The resulting particles have a size of about 10 nm according to HRTEM image. While the structural properties of the CQDs were confirmed by XRD and XPS, and optical behaviors were confirmed by UV–Vis and fluorescence spectroscopies. The electrochemical behavior of the obtained CQDs was tested as electrolyte material for capacitor applications. Experiments were carried out in three different operating potential windows in the 0–2 V range, and CQDs electrolytes exhibited high capacitive effect in symmetrical capacitors. However, the cyclic voltammetry (CV) analyses revealed that the CQDs electrolytes displayed a full supercapacitor electrolyte feature in the 0–0.5 V range. The CQDs electrolytes have a promising material for technological and industrial applications with their unique redox performance and high capacitive effect.

1. Introduction

Fluorescent and semiconductor CQDs have become very popular among carbonaceous materials [1,2]. These materials were discovered for the first time by Xu and his coworkers during the synthesis and purification of single-walled carbon nanotubes, and named carbon quantum dots for the first time by Sun [3–6]. They are among the most attractive materials of recent decade due to their particle sizes of less than 10 nm and many features that can be developed and adjusted as desired [3–12]. These excellent properties include chemical and photoluminescence stability, wide absorption bands, narrow emission peaks belonging to highly stable materials, high-intensity emission colors, surface modification, biocompatibility, and low toxicity [4,8–12]. Considering the damage caused by traditional heavy metal-based nanoparticles to the environment, it is possible to say that in addition to these excellent properties, they are environmentally friendly and harmless to human health [13–16] These properties allow these materials to be used in many application areas. These applications can be sorted such as bio-sensing, bioimaging, inks for printing techniques, photocatalysts, optoelectronic devices and capacitance measurements [17–22]. In the recent years, many extraction methods have been used for the synthesis of carbon quantum dots, many of which are inexpensive and involve fairly simple reaction pathways [23]. These methods are laser ablation, plasma treatments, arc discharge, electrochemical techniques, combustion/thermal oxidation, microwave irradiation, hydrothermal/acidic oxidation and ultrasonic preparation etc. [4,24–32]. In general, two commonly known routes are followed when obtaining CQDs. These are bottom-up methods based on chemical molecular starting materials such as citric acid and carbohydrates or bottom-down approaches based on fine carbon structures such as graphene, carbon nanotubes and graphite [8,26,29,33–35]. In a natural synthesis method of CQDs and bottom-up approaches, besides hydrothermal or

* Corresponding author.
E-mail address: adem.kocyigit@bilecik.edu.tr (A. Kocyigit).

https://doi.org/10.1016/j.diamond.2023.110275
Received 19 April 2023; Received in revised form 8 July 2023; Accepted 4 August 2023
Available online 6 August 2023

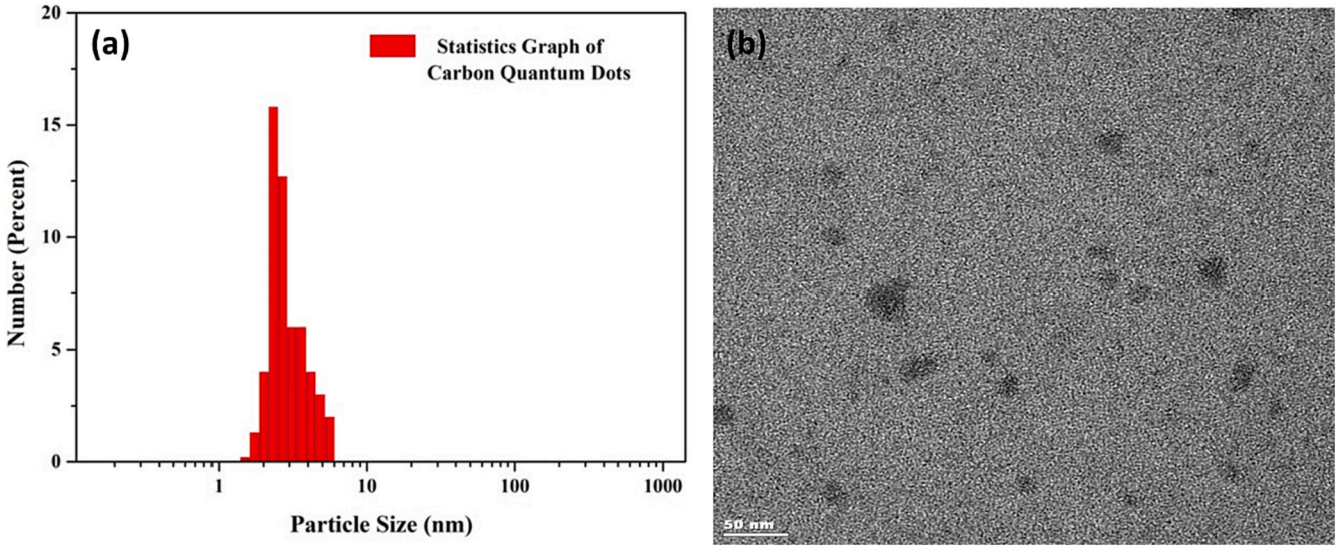

Fig. 1. a) Size histogram and b) the HRTEM image of CQDs.

microwave treatment methods, natural materials, food sources such as garlic, orange, banana, mushrooms, carbohydrates such as fructose and glucose, plants such as bamboo and bergamot can be used [36–43]. Kombucha Fungus is among the natural samples that can be used in these syntheses [44,45].

CQDs provide ultra-small size structures, dispersion within the material, excellent electron transfer properties, and enhanced stronger edge quantum effects [46,47]. With these unique features, CQDs have shown high performance in many technological fields such as energy conversion systems, solar cells, thermoelectric modules, batteries and supercapacitors from past to present [48]. Especially for supercapacitors, which are expected to be an important player in energy storage systems in the future, CQDs performances are of great importance in terms of both industry, technology and literature. It is a remarkable material for supercapacitors with capacitance values ranging from 100 to 600 F/g [48,49].

Although there are many studies on CQDs in the literature, it is not often encountered in experimental studies as an electrolyte material in energy storage systems. Especially, the fact that the CQDs structure provides high performance in terms of ionic conductivity at 2–3 nm levels and has a working mechanism suitable for Lithium and Sodium-ions is of great importance for the examination of the electrolyte performance of CQDs electrolytes [50]. In this study, CQDs synthesized from fermented tea with Kombucha fungus were tested as electrolyte material for capacitor applications. CQDs with higher emission intensity were obtained from the reaction of fermented tea with amine-containing ethylene diamine (EDA) due to its high acidity. The electrolyte materials play an active role in determining the operating voltage window in energy storage systems [51]. We aimed to obtain high specific capacitive performance via increasing the electrode-electrolyte interactions with high-level distribution of the CQDs in the electrolyte materials. The synthesized CQDs were tested in 3 various working potential windows in the 0–2 V range, and they exhibited a promising behavior for technological and industrial applications with their unique redox performance and high capacitive effect.

2. Experimental

2.1. Materials and Synthesis of CQDs

Kombucha tea fungus was fermented in the laboratory after purchasing of Kombucha. Ethylene diamine (99 %, EDA) were purchased from Sigma-Aldrich. Milli-Q water was used in all synthesis and spectroscopic measurements. After fermentation procedure [44,45,52], 50 ml fermented tea was filtered, and 0.2 ml of EDA was added into the tea [53]. The mixed solution was stirred vigorously for 5 h. When the formation of CQDs was seen from the green emission under UV-light, the obtained product was filtered with a 0.2 mm pore filter [44,45]. Thus, synthesizing of CQDs were completed for characterization and testing as an electrolyte material for supercapacitor applications.

2.2. Characterization

Fluorescence emissions of the CQDs were measured by using Perkin Elmer LS 55 brand luminescence spectrometer. UV absorption measurements were obtained by using a Perkin Elmer Lambda 25 brand UV–Vis Spectrophotometer. A JEOL JEM 2100 FHRTEM brand high-resolution tunneling electron microscopy (HRTEM) was used to image the particles. Particle sizes were determined with MALVERN/ DLS MPT2 brand dynamic light scattering (DLS). Bruker Advance D8 brand X-ray diffractometer (XRD) was employed to determine the crystallinity of CQDs. The elemental composition of CQDs was studied using Thermo Scientific K-Alpha X-ray photoelectron spectroscopy (XPS) equipped with a monochromatic Al/Kα as the X-ray source.

2.3. Electrochemical Measurements

The electrolyte properties of CQDs materials were investigated with the Gamry brand model 1010-E Potentiostat system. The 3-electrode method was applied to measure electrolyte properties with cyclic voltammetry (CV) measurements. The CV measurements were carried out at a constant scan speed of 100, 200, 400, 800, 1200, 1600 and 2000 mV/s. The CV measurements were carried out as 3 cycles to observe any anomalies. However, only one CV cycle data has been given in the result section to avoid data analyses confusion. While the platinum foils were used as an electrode (working and counter) as well as current collector, Ag/AgCl electrode was employed as a reference electrode. The cycle life capacitance measurements were performed under 200 mV/s constant scanning speed in a range of 0–0.5 V, 0–1 V and 0–2 V for 100 cycles. Then, the capacitance values of the samples are calculated with Eq. (1) in reference to CV results [54].

$$C = \frac{\int I dV}{2m\Delta V v} \tag{1}$$

In Eq. (1), I is current, m is electrolyte active material weight, υ is scan rate, and ΔV is voltage range.

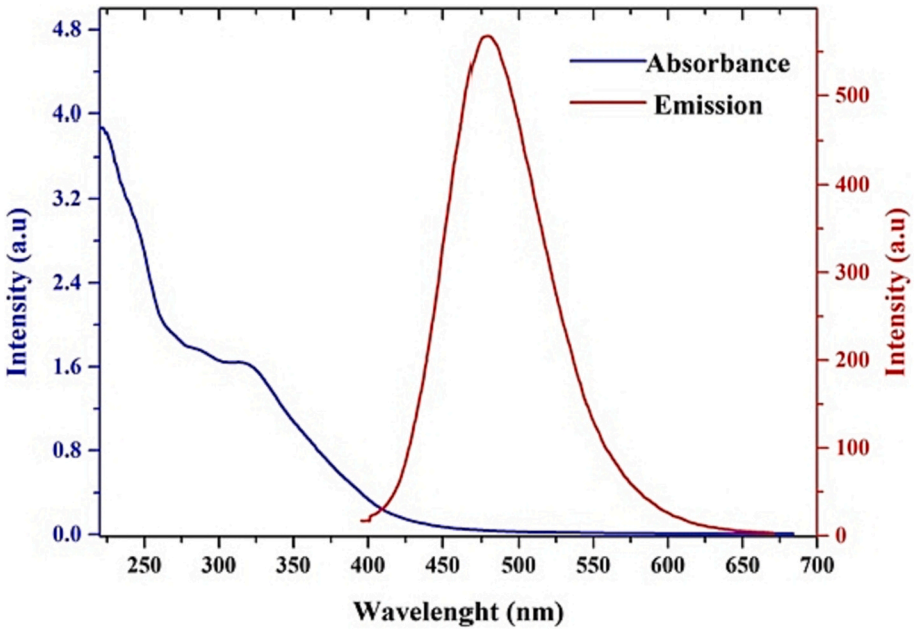

Fig. 2. Fluorescence and UV–Vis absorption spectra.

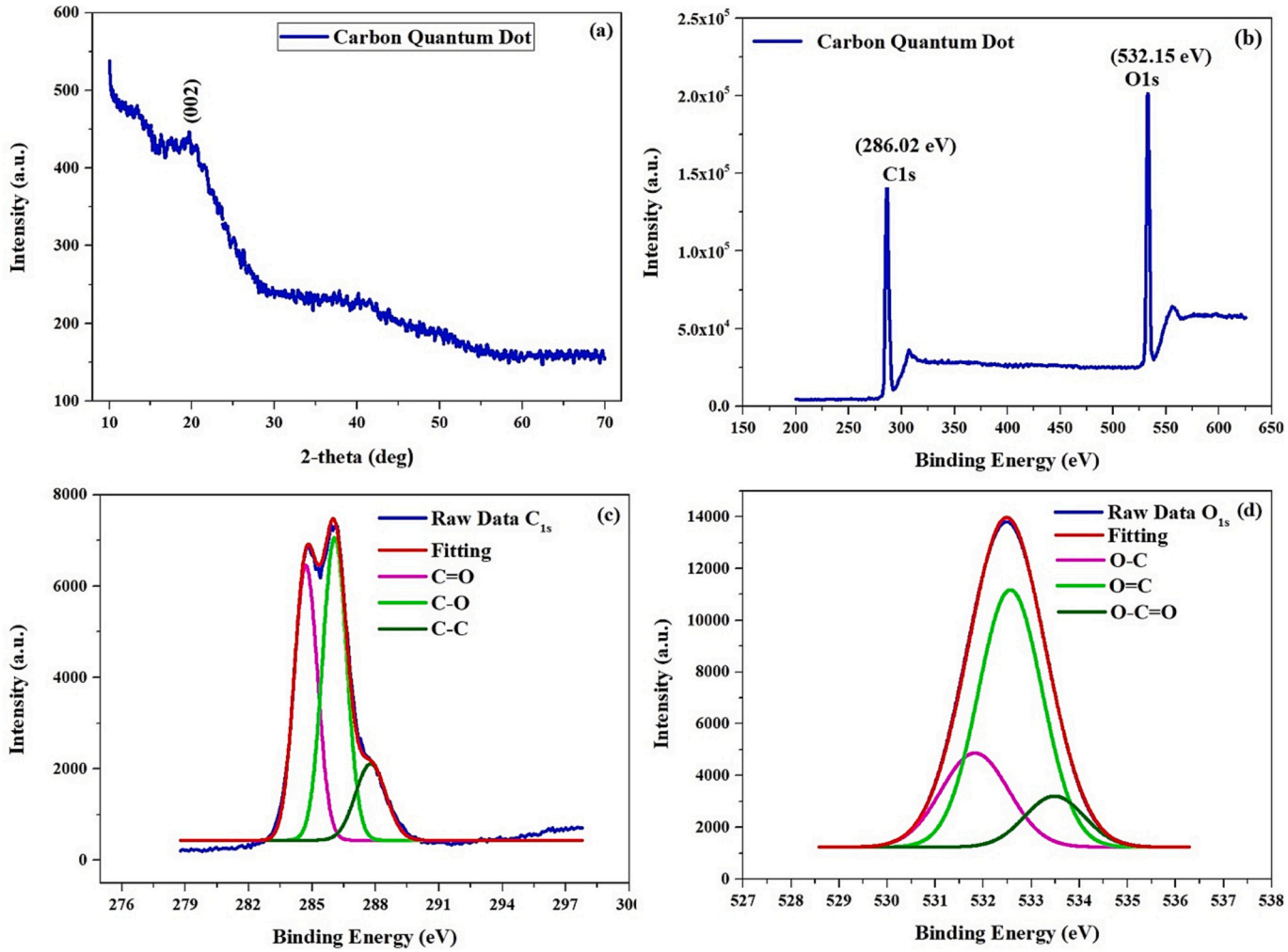

Fig. 3. a) XRD and b) XPS survey spectrum and XPS deconvolutions c) C1s, d) O1s for CQDs.

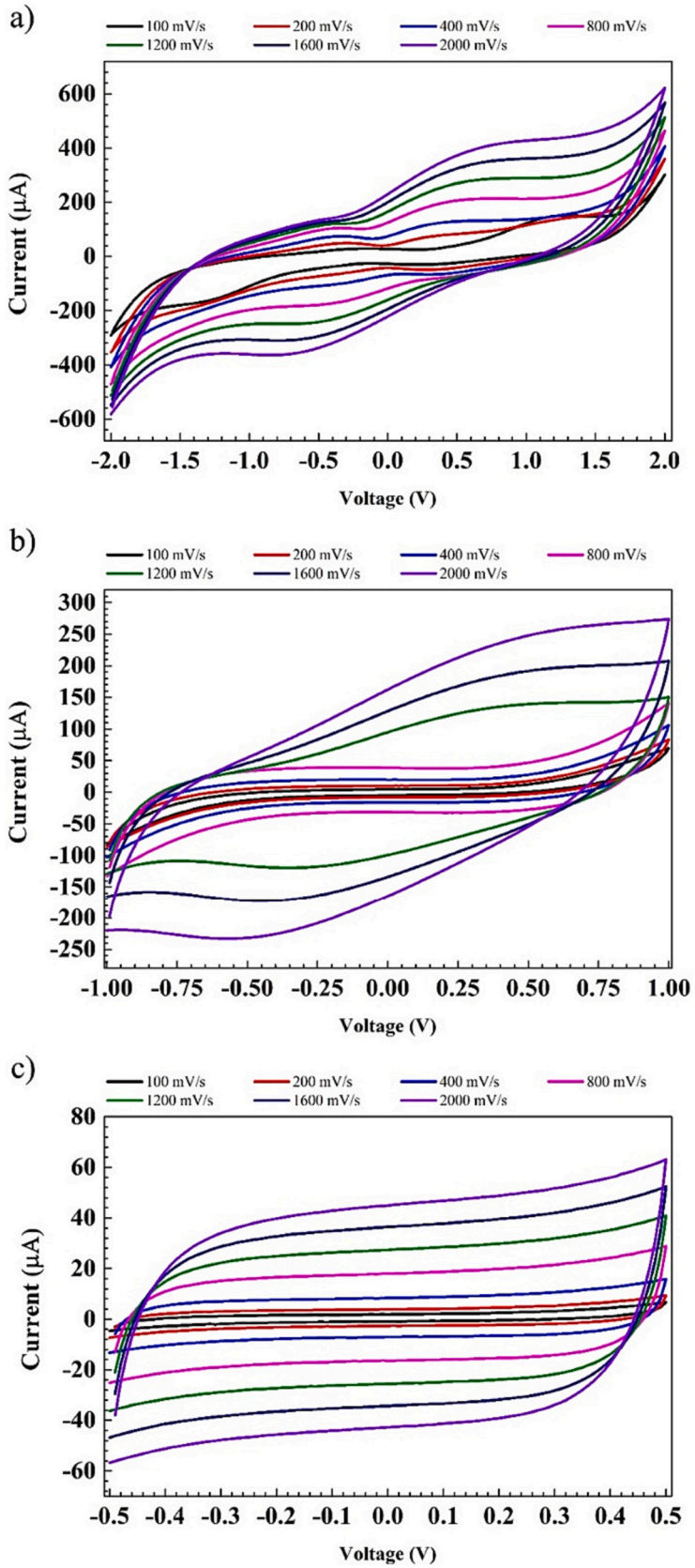

Fig. 4. Permanent capacitive plateaus and redox reaction observations at CV analyses. a) 0–2 V range, b) 0–1 V range, and c) 0–0.5 V range.

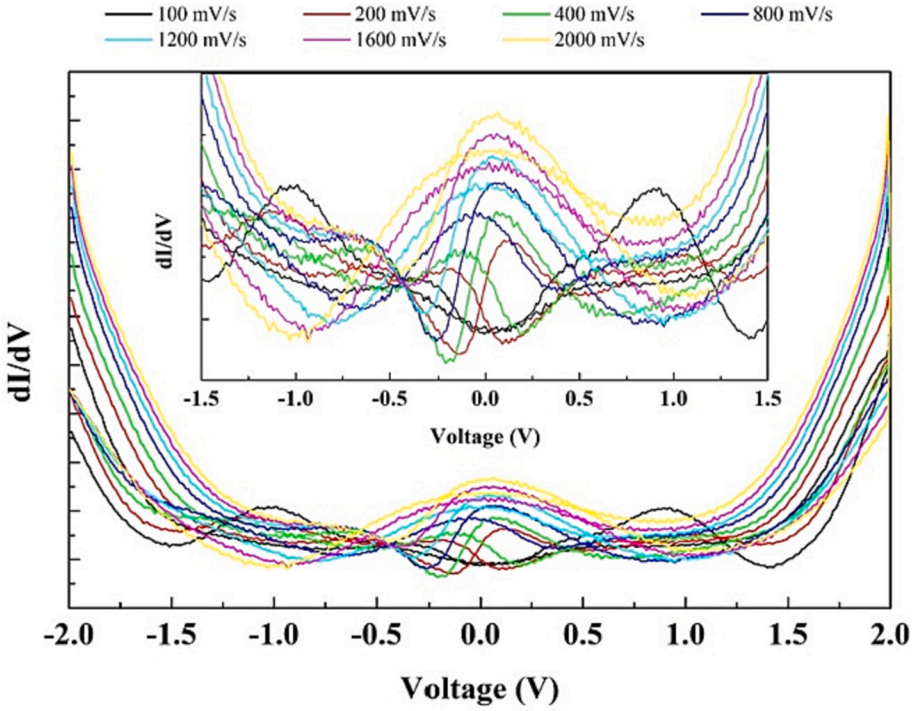

Fig. 5. dI/dV analysis of CQDs samples between ±2 V.

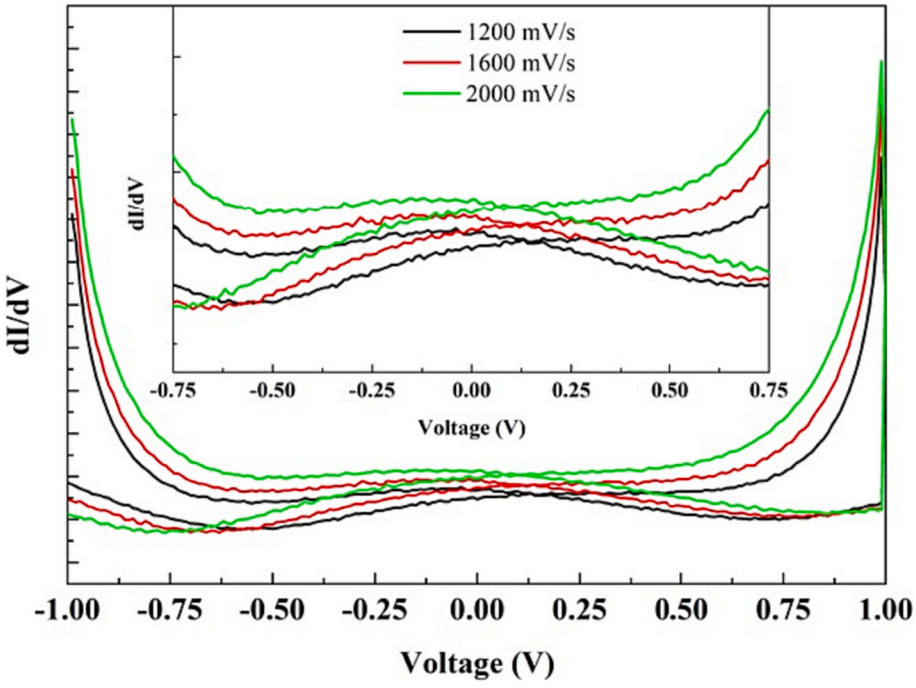

Fig. 6. dI/dV analysis of CQDs samples between ±1 V.

3. Results and discussion

3.1. Optical and Structural Characterizations of CQDs

To demonstrate the size distribution of the CQDs, size measurements of CQDs solution in an aqueous state were obtained by DLS, and for investigating the morphologies of CQDs, the measurements were performed by HRTEM. As seen in Fig. 1a and b, the graph obtained from the DLS and HRTEM images of the obtained CQDs show the particles have a near spherical and monodisperse size with around 10 nm approximately. It can also be seen from Fig. 1b that the prepared particles are well distributed on the surface. The sizes of the small particles in Fig. 1b which is well consistent with that of the CQDs in Fig. 1a [55–57].

Fig. 2 shows the UV–Vis absorption and fluorescence spectra of CQDs. The obtained CQDs have strong absorbance of around 200–250 nm, which is attributed to the conjugated C═C units. This large peak is related to π-π* transition of aromatic sp^2 domains [58]. The other maximum absorbance peak at around 330–340 nm is ascribed to

Table 1
Redox peak voltages in the range of ±1 V and ± 2 V.

±2 V range			±1 V range		
Scan rate (mV/s)	Peak voltage		Scan rate (mV/s)	Peak voltage	
	1. Peak	2. Peak		1. Peak	2. Peak
100	0.490	0.900	100	–	–
200	0.130	1.020	200	–	–
400	0.080	–	400	–	–
800	0.050	–	800	–	–
1200	0.048	–	1200	0.120	–
1600	0.043	–	1600	0.100	–
2000	0.028	–	2000	0.080	–

transitions due to carbonyl or amine functional groups in the structure, and it was related to the n → π* electron transition in the bond of oxygen or nitrogen-containing which is consistent with previous studies [59–62]. Optically to characterize synthesized CQDs, fluorescence spectroscopy was also used, and the obtained emission spectra CQDs showed an emission peak at around 475 nm according to Fig. 2 with blue-colored fluorescence for excitation wavelength at 360 nm [63].

The crystalline structure of CQDs was studied by XRD, and elemental analysis and chemical bonding structures of CQDs were investigated by XPS. While the Fig. 3a shows XRD pattern of the CQDs, Fig. 3b–d indicate XPS survey spectrum and deconvolutions. According to the X-ray diffraction (XRD) pattern, Fig. 3a displays only one sharp peak at about $2\theta = 20^{\circ}$ due to the CQDs [64,65]. The obtained wide diffraction peak also at around 42° can be attributed to CQDs, and it is in good agreement with the previously reported results in the literature [66,67]. The full-scale XPS survey scanning was performed to elucidate the composition of carbon dots. Two peaks, which are predominantly seen at 286.02 eV and 533.15 eV in Fig. 3b, belong to C and O elements, respectively, and it highlights that the amount of these elements in the structure of the material is quite high. As seen in Fig. 3c and d, the high resolution C1s spectrum displays three peaks at 284.6 eV, 286.0 eV and 287.7 eV belonging to C═O, C—O and C—C bindings, respectively. XPS spectrum of O1s (Fig. 3d) revealed three different unit moieties; O—C bonds (581.82 eV), O═C bonds (532.56 eV) and, O–C=O bonds (533.48 eV), respectively [63,68,69].

3.2. Electrochemical analysis

The electrolyte properties analyze for electrochemical capacitors was started with CV measurements. The CV analyzes were performed at ±0.5 V, ±1 V and ±2 V ranges to determine which voltage ranges could be ideal for capacitive applications. Fig. 4a–c shows the CV results obtained at different scan rates for the CQDs electrolyte samples. CV analyzes of CQDs showed permanent capacitive currents in 3 different voltage region scans. Also, some redox reaction peaks were observed with Faradic current in the ±1 V and ±2 V ranges.

Fig. 4a shows the current-voltage changes in the ±2 V range. Some shifts occurred in some redox peaks formed in the material especially at scanning speeds after the 100 mV/s. In fact, there were shifts in the redox peak voltage values that occurred in fast scanning with increasing scanning speed. The shift of the redox peaks towards 0 V depending on the increasing scanning rate indicates that ionic diffusion can occur more easily at high rates in the range of ±2 V. Applying a higher voltage

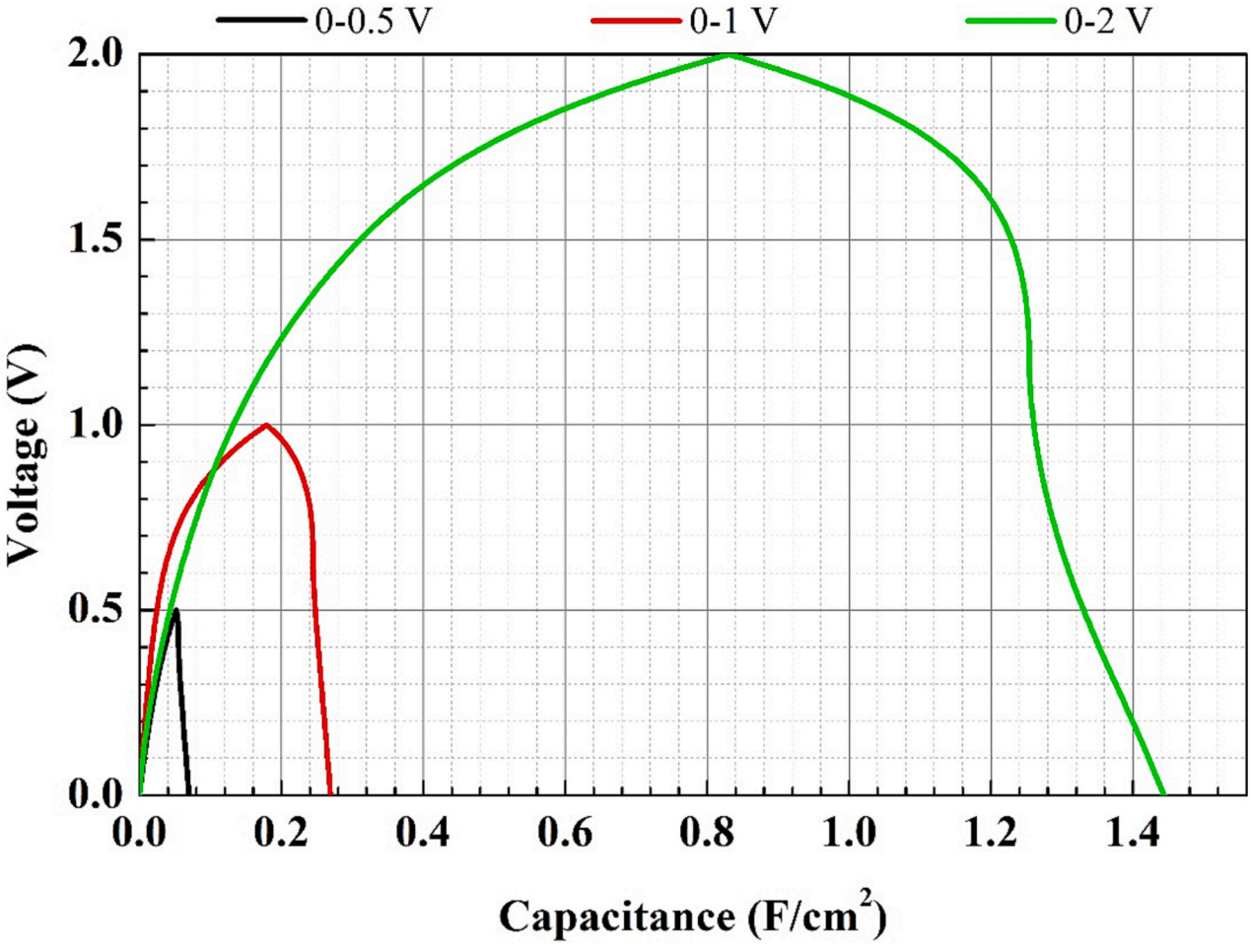

Fig. 7. First cycle capacitive performance of CQDs materials.

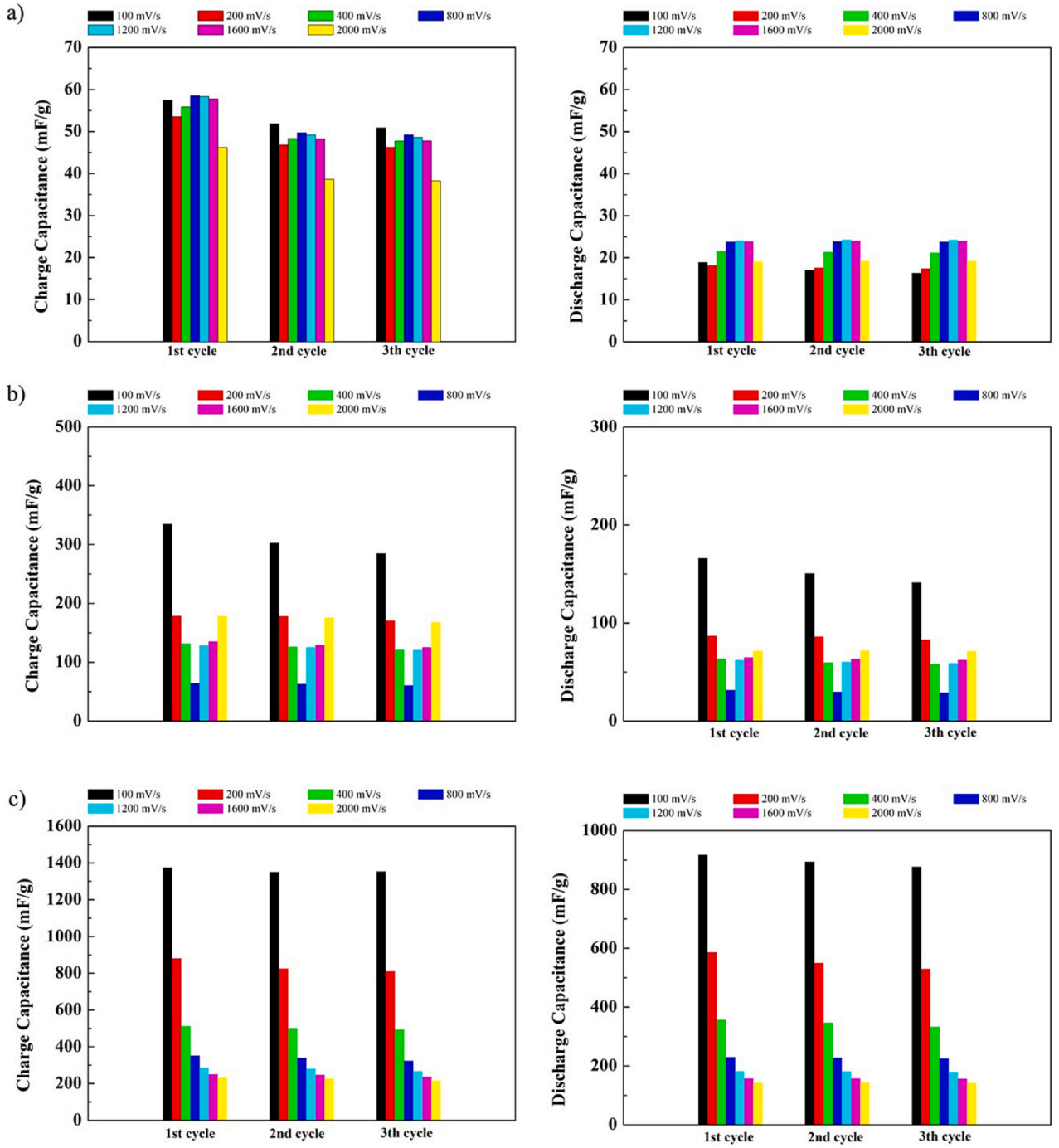

Fig. 8. First 3 cycles performances of CQDs electrolyte for different CV rates. a) 0–0.5 V charge and discharge capacitance, b) 0-1 V charge and discharge capacitance, c) 0-2 V charge and discharge capacitance.

for the CQDs electrolyte as the ±2 V range, compared to other range measurements, it may have resulted in faster debonding or bonding properties in CQDs materials.

A similar situation was observed in CV measurements at ±1 V range (Fig. 4b). The interesting situation in the range of ±1 V was that while redox reactions were not activated up to 800 mV/s scanning speed, the currents from redox peaks contributed to Faradic currents in the range of 1200–2000 mV/s scanning speeds. While the formation of redox peaks was observed in the range of ±2 V under normal conditions, their existence after scanning at a certain speed in the range of ±1 V indicated that there was a threshold voltage value for some reactions in the CQDs. In addition, the material also showed adaptation to high-speed scanning in the range of ±1 V.

Fig. 4c shows the CV measurements for the ±0.5 V range. In particular, the characteristic rectangular CV shape of the CQDs electrolyte in the range of ±0.5 V, stood out as a very remarkable result for supercapacitor productions. In ±0.5 V range, only Faradic currents were observed, but redox peak was not observed due to the increased scanning speed. This indicates that redox reactions may occur in the material, especially after ±1 V.

Figs. 5 and 6 show dI/dV analysis based on ±1 V and ± 2 V CV measurements. The dI/dV analysis can allow being easily observation of the changes in the CV plane, and the voltage values of the redox peaks can be determined with this analysis. Table 1 was prepared according to

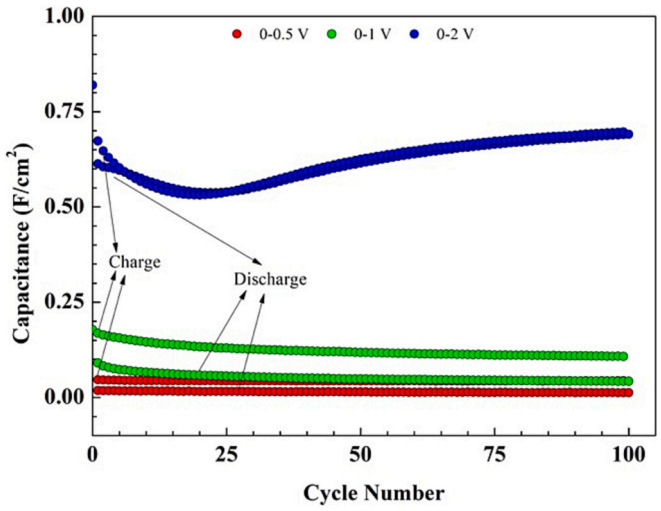

Fig. 9. Redox effects on cycle-life performance of CQDs electrolyte.

the data obtained from the dI/dV analyzes and the voltage values of the redox peaks. When the redox peaks occurring in the range of ±2 V were examined, two different redox formations were observed at 100 and 200 mV/s scanning rates. After these scan speeds, the second redox peaks disappeared, and only capacitive currents were observed. The main reason for the disappearance of these peaks at high velocities is that the activated ions at ~1 V are prevented from ionizing in the structure trying to adapt to high velocities. On the other hand, in the first redox peak occurring in the 100–2000 mV/s scan rates, it is seen that as the scanning speed increased, the ionization peak shifts occurred towards 0 V. This indicates that ions in the 0–0.4 V range can diffuse more easily in the material and that the material is more prone to energy storage at these speeds. A similar situation can be seen in dI/dV calculations for the ±1 V range. In the ±1 V range, the measurements between 1200 and 2000 mV/s scan rates, the redox peak formations and shifts towards 0 V level was observed. The redox peak was obtained as 0.120 V at 1200 mV/s scan rate, and decreased to 0.080 V at 2000 mV/s scan rate. Similar to the ±2 V range, the material can adapt to high-speed charge-discharge processes in the ±1 V range (Table 1).

Fig. 7 shows the first charge-discharge capacitance performance for various voltage ranges. It is seen that the charge-discharge values are generally below the Farad level and CQDs electrolytes can store energy at milli-Farad levels. Although this situation does not comply with the definition of supercapacitor, the material shows a full supercapacitive electrolyte feature, especially in the 0–0.5 V range. Fig. 7 also indicates the effects of the redox peaks formed in the measurements in the 0–1 and 0–2 V range on the charge-discharge patterns. Another remarkable thing is that higher capacitance is obtained in measurements made in the 0-2 V range compared to other voltage ranges. The main reason for this is that the material has 2 different redox reactions at a scanning speed of 200 mV/s. In this way, CQDs can store more energy in its structure.

After examining the first charge-discharge cycles at 200 mV/s constant scan rate, the capacitive performances of the CQDs electrolyte at different scan rates were analyzed for the first 3 cycles Fig. 8a, b and c display first 3 cycles performances of the CQDs for 0–0.5 V, 0–1 V and 0–2 V ranges charge and discharge capacitance values, respectively. Under normal conditions, batteries and capacitors store and use lower energy under high currents and voltages. This situation in CQDs electrolytes was observed differently. The capacitance decreased with 200 mV/s scan speed after 100 mV/s scan speed in the 0–0.5 V charging range, but it increased at 400 mV/s and increasing voltage scanning speeds. This increase also reached the highest level at 800 mV/s. However, this situation has been observed differently as discharge capacitance. While lower capacitance values were obtained at 100 and 200 mV/s scanning speeds compared to other scanning speeds, the highest discharge capacitance values were obtained at 800–1600 mV/s scanning speeds. Although the lowest capacitance values were obtained in the range of 0–0.5 V, this situation revealed the ideal operation feature of CQDs electrolyte material under high charge-discharge speeds. Fig. 8b shows charge-discharge performances in the 0-1 V range. In this range, the capacitance values decreased with increasing scanning speed as expected, but there was an increase in the capacitance values with the contribution of the redox peaks that appeared at the 1200–2000 mV/s scan speeds. This condition can be attributed to the redox reactions at high speeds. This also reveals that the CQDs electrolyte material has a better operating voltage range than 0–0.5 V and increases its industrial application compatibility with the charge-discharge rate. Fig. 8c shows charge-discharge performances in the 0-2 V range. Although the highest capacitance values were obtained in the 0-2 V range, a decrease was observed in the capacitance values depending on the increasing scanning speed. This shows that the material is not very efficient in high-speed charge-discharge operations in the 0-2 V range.

Fig. 9 shows the cycle-life analyzes performed at 0–0.5, 0–1 and 0–2 V ranges. As a result of the analyzes performed at a constant scanning speed of 200 mV/s, the highest capacitance values were obtained in the 0-2 V range. In addition, the values in which the charge-discharge capacitance values were closest to each other during 100 cycles were obtained in the range of 0–2 V. Moreover, the capacitive performance in the 0-2 V range decreased during the first 25 cycles, and then recovered and achieved the ideal capacitive performance. The capacity retention rates of the CQDs electrolyte material during 100 cycles are given in Table 2. Especially with a retention value of −12.8 %, CQDs positively increased the discharge performance at the end of 100 cycles in the

Table 3
CQDs electrolyte comparison with conventional electrolytes.

Electrolyte	Capacitance	Working potential	Reference
NaCl	0.11 mF/cm^2	0–0.3 V	
	0.14 mF/cm^2	0–0.5 V	[70]
	0.35 mF/cm^2	0–1 V	
KOH (with metal oxide electrodes)	124.80 mF/g	(−1)-0 V	[71]
LiOH (with metal oxide electrodes)	74.20 mF/g	0–0.6 V	[71]
NaOH (with metal oxide electrodes)	187.10 mF/g	0.1–0.4 V	[71]
Green synthesized CQDs	18 mF/cm^2	0–0.5 V	This Study
	91 mF/cm^2	0–1 V	This Study
	613 mF/cm^2	0–2 V	This Study

Table 2
Capacity retention rates of CQDs electrolyte.

Voltage range (V)	1. cycle		25. cycle		50. cycle		100.cycle		Retention (%)	
	Ch.	Dch.	Ch.	Dch.	Ch.	Dch.	Ch.	Dch.	Ch.	Dch.
0–0.5	52	18	43	16	43	14	43	12	17.3	33.3
0–1	178	91	129	56	118	48	107	42	39.8	53.8
0–2	823	613	539	536	622	612	697	692	15.3	−12.8

Ch: Charge Capacitance (mF/cm^2); Dch: Discharge Capacitance (mF/cm^2)

range of 0–2 V. A negative retention value indicates an increase in capacitance at the end of 100 cycles. The capacity retention values of the capacitors were calculated according to these specific capacitance values. The capacity retention formula is:

$$Retention\ (\%) = \frac{C_0 - C_n}{C_0} x100 \quad (2)$$

where C_0 is the first-cycle capacitance value (F/g) and C_n is the last cycle capacitance value (F/g).

The obtained different performances of the same material at different voltage ranges are due to the differences in the chemical structure of the material. Also, it is thought that the capacitive performance CQDs electrolytes changes depending on the solid electrolyte interface (SEI) layer formation under different potentials. In addition, when the current peak values are examined depending on the CV analysis, it is thought that the electrolyte has more current on the anodic section, and this also may explain that the SEI layer on the cathode is more effective. Moreover, while the redox active ions formed in the 0–1 V range are diffusing towards the anode pole during charging, it cannot be realized with full efficiency in the opposite direction during discharge. In the 0–2 V range, this situation is higher and shows that the transfer of redox active ions for charge-discharge can be achieved more easily. Moreover, the material may play an active role in providing high capacitance during long cycles by adapting to these ion transfers over long cycles.

Table 3 shows the capacitive performance comparison of CQDs electrolyte compared to other conventional electrolytes. The CQDs electrolytes, which form the basis of our study, are clearly superior to other conventional electrolytes in terms of both working potential and capacity. Moreover, the capacitance values of the most preferred supercapacitor electrolytes such as KOH, LiOH and NaOH have a capacitive contribution (with electrode redox reactions) in metal oxide electrodes. This situation also provides an advantage in terms of our study in which Pt-foil electrodes that do not cause any redox reaction were used. In other words, these values were reached by keeping the electrode contribution to the capacitance values obtained at minimal levels.

Within the scope of the study, although mF level capacitance is obtained from green synthesized CQDs electrolytes, it is known that the type of electrode contributes to the high or low capacitance values. In this study with platinum foils, the electrolyte effect of CQDs was investigated by minimizing the electrode contribution. Although a normal capacitor capacitance performance is obtained in the CQDs symmetrical capacitor produced with platinum foils, it is concluded that high-performance supercapacitors can be produced with different electrodes that can be combined with CQDs electrolyte. In particular, it is thought that supercapacitors with higher capacitance can be produced with an electrode with a higher pore structure or a redox-active material with a discharge capacitance of 692 mF/cm^2 reached in the 0–2 V operating range. Considering that the obtained values are also the result of charge-discharge at high speeds, it has been concluded that green synthesized CQDs electrolytes can be used for capacitor applications.

4. Conclusions

CQDs were obtained with environmentally friendly materials in a simple and easy way. In this synthesis route, tea samples left to fermentation with kombucha, an aquatic mushroom species, were preferred as carbon source. When the commonly used characterization techniques for the obtained CQDs nanomaterials were used, it was observed that CQDs had high emission and uniform particle size according to the obtained results. Successful results were obtained when the capacitors were examined in terms of their electrochemical behavior. Accordingly, experiments were carried out in three different operating potential windows in the 0–2 V range, and it was found promising that CQDs electrolytes have a high capacitive effect in symmetrical capacitors produced with platinum foils, where the possible redox contribution from the electrodes can be minimized. Moreover, it is predicted that supercapacitor performance can be achieved in new capacitor derivatives where different types of electrodes can be used with CQDs electrolytes. CQDs with their unique redox performance is expected to be the hope for many technological and industrial applications.

Funding

The authors declare that no funds, grants, or other support were received during the preparation of this manuscript.

CRediT authorship contribution statement

Canan Başlak Synthesized CQDs nanoparticles. Canan Başlak and M. Okan Erdal obtained characterization measurements. Canan Başlak, M. Okan Erdal and Serkan Demirel wrote the main manuscript text. Adem Kocyigit and Murat Yıldırım organized study, edited and reviewed manuscript.

Declaration of competing interest

The authors declare that they have no known competing financial interests or personal relationships that could have appeared to influence the work reported in this paper.

Data availability

Data will be made available on request.

References

[1] N. Azam, M. Najabat Ali, T. Javaid Khan, Carbon quantum dots for biomedical applications: Review and analysis, Front. Mater. 8 (2021), https://doi.org/10.3389/fmats.2021.700403.
[2] P.K. Yadav, S. Chandra, V. Kumar, D. Kumar, S.H. Hasan, Carbon quantum dots: Synthesis, structure, properties, and catalytic applications for organic synthesis, Catalysts 13 (2023) 422, https://doi.org/10.3390/catal13020422.
[3] F. Du, M. Zhang, X. Li, J. Li, X. Jiang, Z. Li, Y. Hua, G. Shao, J. Jin, Q. Shao, M. Zhou, A. Gong, Economical and green synthesis of bagasse-derived fluorescent carbon dots for biomedical applications, Nanotechnology. 25 (2014), 315702, https://doi.org/10.1088/0957-4484/25/31/315702.
[4] Y.-P. Sun, B. Zhou, Y. Lin, W. Wang, K.A.S. Fernando, P. Pathak, M.J. Meziani, B. A. Harruff, X. Wang, H. Wang, P.G. Luo, H. Yang, M.E. Kose, B. Chen, L.M. Veca, S.-Y. Xie, Quantum-sized carbon dots for bright and colorful photoluminescence, J. Am. Chem. Soc. 128 (2006) 7756–7757, https://doi.org/10.1021/ja062677d.
[5] H. Zhu, X. Wang, Y. Li, Z. Wang, F. Yang, X. Yang, Microwave synthesis of fluorescent carbon nanoparticles with electrochemiluminescence properties, Chem. Commun. (2009) 5118, https://doi.org/10.1039/b907612c.
[6] S. Yao, Y. Hu, G. Li, A one-step sonoelectrochemical preparation method of pure blue fluorescent carbon nanoparticles under a high intensity electric field, Carbon N. Y. 66 (2014) 77–83, https://doi.org/10.1016/j.carbon.2013.08.044.
[7] J. Shen, Q. Li, Y. Zhang, X. She, C.-F. Wang, S. Chen, Nitrogen-doped carbon dots derived from polyamindoamine dendrimer, RSC Adv. 6 (2016) 59702–59707, https://doi.org/10.1039/C6RA12261B.
[8] S. Zhu, J. Zhang, C. Qiao, S. Tang, Y. Li, W. Yuan, B. Li, L. Tian, F. Liu, R. Hu, H. Gao, H. Wei, H. Zhang, H. Sun, B. Yang, Strongly green-photoluminescent graphene quantum dots for bioimaging applications, Chem. Commun. 47 (2011) 6858, https://doi.org/10.1039/c1cc11122a.
[9] Q. Huang, X. Lin, C. Lin, Y. Zhang, S. Hu, C. Wei, A high performance electrochemical biosensor based on cu 2 O–carbon dots for selective and sensitive determination of dopamine in human serum, RSC Adv. 5 (2015) 54102–54108, https://doi.org/10.1039/C5RA05433H.
[10] B. Yin, J. Deng, X. Peng, Q. Long, J. Zhao, Q. Lu, Q. Chen, H. Li, H. Tang, Y. Zhang, S. Yao, Green synthesis of carbon dots with down- and up-conversion fluorescent properties for sensitive detection of hypochlorite with a dual-readout assay, Analyst 138 (2013) 6551, https://doi.org/10.1039/c3an01003a.
[11] A. Zhu, Q. Qu, X. Shao, B. Kong, Y. Tian, Carbon-dot-based dual-emission nanohybrid produces a ratiometric fluorescent sensor for in vivo imaging of cellular copper ions, Angew. Chem., Int. Ed. 51 (2012) 7185–7189, https://doi.org/10.1002/anie.201109089.
[12] A. Jaiswal, S.S. Ghosh, A. Chattopadhyay, One step synthesis of C-dots by microwave mediated caramelization of poly(ethylene glycol), Chem. Commun. 48 (2012) 407–409, https://doi.org/10.1039/C1CC15988G.

[13] S. Zhu, Q. Meng, L. Wang, J. Zhang, Y. Song, H. Jin, K. Zhang, H. Sun, H. Wang, B. Yang, Highly Photoluminescent carbon dots for multicolor patterning, sensors, and bioimaging, Angew. Chem. 125 (2013) 4045–4049, https://doi.org/10.1002/ange.201300519.

[14] L. Tang, R. Ji, X. Cao, J. Lin, H. Jiang, X. Li, K.S. Teng, C.M. Luk, S. Zeng, J. Hao, S. P. Lau, Deep ultraviolet photoluminescence of water-soluble self-passivated graphene quantum dots, ACS Nano 6 (2012) 5102–5110, https://doi.org/10.1021/nn300760g.

[15] A.B. Bourlinos, R. Zbořil, J. Petr, A. Bakandritsos, M. Krysmann, E.P. Giannelis, Luminescent surface quaternized carbon dots, Chem. Mater. 24 (2012) 6–8, https://doi.org/10.1021/cm2026637.

[16] Z. Xie, F. Wang, C. Liu, Organic-inorganic hybrid functional carbon dot gel glasses, Adv. Mater. 24 (2012) 1716–1721, https://doi.org/10.1002/adma.201104962.

[17] L. Cao, X. Wang, M.J. Meziani, F. Lu, H. Wang, P.G. Luo, Y. Lin, B.A. Harruff, L. M. Veca, D. Murray, S.-Y. Xie, Y.-P. Sun, Carbon dots for multiphoton bioimaging, J. Am. Chem. Soc. 129 (2007) 11318–11319, https://doi.org/10.1021/ja073527l.

[18] M. Liong, A.N. Hoang, J. Chung, N. Gural, C.B. Ford, C. Min, R.R. Shah, R. Ahmad, M. Fernandez-Suarez, S.M. Fortune, M. Toner, H. Lee, R. Weissleder, Magnetic barcode assay for genetic detection of pathogens, Nat. Commun. 4 (2013) 1752, https://doi.org/10.1038/ncomms2745.

[19] F. Du, Y. Ming, F. Zeng, C. Yu, S. Wu, A low cytotoxic and ratiometric fluorescent nanosensor based on carbon-dots for intracellular pH sensing and mapping, Nanotechnology. 24 (2013), 365101, https://doi.org/10.1088/0957-4484/24/36/365101.

[20] H. Li, X. He, Z. Kang, H. Huang, Y. Liu, J. Liu, S. Lian, C.H.A. Tsang, X. Yang, S.-T. Lee, Water-soluble fluorescent carbon quantum dots and photocatalyst design, Angew. Chem., Int. Ed. 49 (2010) 4430–4434, https://doi.org/10.1002/anie.200906154.

[21] Q. Wang, X. Huang, Y. Long, X. Wang, H. Zhang, R. Zhu, L. Liang, P. Teng, H. Zheng, Hollow luminescent carbon dots for drug delivery, Carbon N. Y. 59 (2013) 192–199, https://doi.org/10.1016/j.carbon.2013.03.009.

[22] X. Guo, C.-F. Wang, Z.-Y. Yu, L. Chen, S. Chen, Facile access to versatile fluorescent carbon dots toward light-emitting diodes, Chem. Commun. 48 (2012) 2692, https://doi.org/10.1039/c2cc17769b.

[23] H. Xu, X. Yang, G. Li, C. Zhao, X. Liao, Green synthesis of fluorescent carbon dots for selective detection of Tartrazine in food samples, J. Agric. Food Chem. 63 (2015) 6707–6714, https://doi.org/10.1021/acs.jafc.5b02319.

[24] X. Xu, R. Ray, Y. Gu, H.J. Ploehn, L. Gearheart, K. Raker, W.A. Scrivens, Electrophoretic analysis and purification of fluorescent single-walled carbon nanotube fragments, J. Am. Chem. Soc. 126 (2004) 12736–12737, https://doi.org/10.1021/ja040082h.

[25] J. Wang, C.-F. Wang, S. Chen, Amphiphilic egg-derived carbon dots: rapid plasma fabrication, pyrolysis process, and multicolor printing patterns, Angew. Chem., Int. Ed. 51 (2012) 9297–9301, https://doi.org/10.1002/anie.201204381.

[26] Q.-L. Zhao, Z.-L. Zhang, B.-H. Huang, J. Peng, M. Zhang, D.-W. Pang, Facile preparation of low cytotoxicity fluorescent carbon nanocrystals by electrooxidation of graphite, Chem. Commun. (2008) 5116, https://doi.org/10.1039/b812420e.

[27] J.-M. Liu, L. Lin, X.-X. Wang, S.-Q. Lin, W.-L. Cai, L.-H. Zhang, Z.-Y. Zheng, Highly selective and sensitive detection of Cu2+ with lysine enhancing bovine serum albumin modified-carbon dots fluorescent probe, Analyst. 137 (2012) 2637, https://doi.org/10.1039/c2an35130g.

[28] S.N. Baker, G.A. Baker, Luminescent carbon nanodots: emergent nanolights, Angew. Chem., Int. Ed. 49 (2010) 6726–6744, https://doi.org/10.1002/anie.200906623.

[29] J. Zhou, C. Booker, R. Li, X. Zhou, T.-K. Sham, X. Sun, Z. Ding, An electrochemical avenue to blue luminescent nanocrystals from multiwalled carbon nanotubes (MWCNTs), J. Am. Chem. Soc. 129 (2007) 744–745, https://doi.org/10.1021/ja0669070.

[30] H. Liu, T. Ye, C. Mao, Fluorescent carbon nanoparticles derived from candle soot, Angew. Chem. 119 (2007) 6593–6595, https://doi.org/10.1002/ange.200701271.

[31] S. Liu, J. Tian, L. Wang, Y. Zhang, X. Qin, Y. Luo, A.M. Asiri, A.O. Al-Youbi, X. Sun, Hydrothermal treatment of grass: a low-cost, green route to nitrogen-doped, carbon-rich, photoluminescent polymer nanodots as an effective fluorescent sensing platform for label-free detection of cu(II) ions, Adv. Mater. 24 (2012) 2037–2041, https://doi.org/10.1002/adma.201200164.

[32] J. Joseph, A.A. Anappara, Microwave-assisted hydrothermal synthesis of UV-emitting carbon dots from tannic acid, New J. Chem. 40 (2016) 8110–8117, https://doi.org/10.1039/C6NJ02107G.

[33] S. Qu, X. Wang, Q. Lu, X. Liu, L. Wang, A biocompatible fluorescent ink based on water-soluble luminescent carbon nanodots, Angew. Chem., Int. Ed. 51 (2012) 12215–12218, https://doi.org/10.1002/anie.201206791.

[34] H. Peng, J. Travas-Sejdic, Simple aqueous solution route to luminescent carbogenic dots from carbohydrates, Chem. Mater. 21 (2009) 5563–5565, https://doi.org/10.1021/cm901593y.

[35] S. Mohapatra, S. Sahu, N. Sinha, S.K. Bhutia, Synthesis of a carbon-dot-based photoluminescent probe for selective and ultrasensitive detection of Hg 2+ in water and living cells, Analyst. 140 (2015) 1221–1228, https://doi.org/10.1039/C4AN01386G.

[36] Y. Xu, J. Liu, C. Gao, E. Wang, Applications of carbon quantum dots in electrochemiluminescence: a mini review, Electrochem. Commun. 48 (2014) 151–154, https://doi.org/10.1016/j.elecom.2014.08.032.

[37] Z. Li, S. Guo, Z. Yuan, C. Lu, Carbon quantum dot-gold nanocluster nanosatellite for ratiometric fluorescence probe and imaging for hydrogen peroxide in living cells, Sensors Actuators B Chem. 241 (2017) 821–827, https://doi.org/10.1016/j.snb.2016.10.134.

[38] C. Wang, Z. Xu, H. Cheng, H. Lin, M.G. Humphrey, C. Zhang, A hydrothermal route to water-stable luminescent carbon dots as nanosensors for pH and temperature, Carbon N. Y. 82 (2015) 87–95, https://doi.org/10.1016/j.carbon.2014.10.035.

[39] M. Xu, W. Zhang, Z. Yang, F. Yu, Y. Ma, N. Hu, D. He, Q. Liang, Y. Su, Y. Zhang, One-pot liquid-phase exfoliation from graphite to graphene with carbon quantum dots, Nanoscale. 7 (2015) 10527–10534, https://doi.org/10.1039/C5NR02198G.

[40] Q. Ye, F. Yan, D. Shi, T. Zheng, Y. Wang, X. Zhou, L. Chen, N, B-doped carbon dots as a sensitive fluorescence probe for Hg 2+ ions and 2,4,6-trinitrophenol detection for bioimaging, J. Photochem. Photobiol. B Biol. 162 (2016) 1–13, https://doi.org/10.1016/j.jphotobiol.2016.06.021.

[41] M. Xue, L. Zhang, M. Zou, C. Lan, Z. Zhan, S. Zhao, Nitrogen and sulfur co-doped carbon dots: a facile and green fluorescence probe for free chlorine, Sensors Actuators B Chem. 219 (2015) 50–56, https://doi.org/10.1016/j.snb.2015.05.021.

[42] J. Yu, N. Song, Y.-K. Zhang, S.-X. Zhong, A.-J. Wang, J. Chen, Green preparation of carbon dots by Jinhua bergamot for sensitive and selective fluorescent detection of Hg2+ and Fe3+, Sensors Actuators B Chem. 214 (2015) 29–35, https://doi.org/10.1016/j.snb.2015.03.006.

[43] Y. Liu, Y. Zhao, Y. Zhang, One-step green synthesized fluorescent carbon nanodots from bamboo leaves for copper(II) ion detection, Sensors Actuators B Chem. 196 (2014) 647–652, https://doi.org/10.1016/j.snb.2014.02.053.

[44] Ç. Kırbıyık, A. Toprak, C. Başlak, M. Kuş, M. Ersöz, Nitrogen-doped CQDs to enhance the power conversion efficiency of perovskite solar cells via surface passivation, J. Alloys Compd. 832 (2020), 154897, https://doi.org/10.1016/j.jallcom.2020.154897.

[45] A.N.K. Canan Baslak, New optical sensor based on pillar[5]arene-carbon quantum dot composite material, in: III. Int. Sci. Vocat. Stud. Congr, 2019, pp. 34–37.

[46] Q. Sun, Z. Yu, R. Jiang, Y. Hou, L. Sun, L. Qian, F. Li, M. Li, Q. Ran, H. Zhang, CoP QD anchored carbon skeleton modified CdS nanorods as a co-catalyst for photocatalytic hydrogen production, Nanoscale. 12 (2020) 19203–19212, https://doi.org/10.1039/D0NR05268J.

[47] H. Xu, J. Yan, X. She, L. Xu, J. Xia, Y. Xu, Y. Song, L. Huang, H. Li, Graphene-analogue carbon nitride: novel exfoliation synthesis and its application in photocatalysis and photoelectrochemical selective detection of trace amount of cu 2+, Nanoscale. 6 (2014) 1406–1415, https://doi.org/10.1039/C3NR04759H.

[48] Q. Li, H. Cheng, X. Wu, C.-F. Wang, G. Wu, S. Chen, Enriched carbon dots/graphene microfibers towards high-performance micro-supercapacitors, J. Mater. Chem. A 6 (2018) 14112–14119, https://doi.org/10.1039/C8TA02124D.

[49] J. Wei, C. Ding, P. Zhang, H. Ding, X. Niu, Y. Ma, C. Li, Y. Wang, H. Xiong, Robust negative electrode materials derived from carbon dots and porous hydrogels for high-performance hybrid supercapacitors, Adv. Mater. (2018) 1806197, https://doi.org/10.1002/adma.201806197.

[50] C. Ma, K. Dai, H. Hou, X. Ji, L. Chen, D.G. Ivey, W. Wei, High ion-conducting solid-state composite electrolytes with carbon quantum dot nanofillers, Adv. Sci. 5 (2018) 1700996, https://doi.org/10.1002/advs.201700996.

[51] B. Pal, S. Yang, S. Ramesh, V. Thangadurai, R. Jose, Electrolyte selection for supercapacitive devices: a critical review, Nanoscale Adv. 1 (2019) 3807–3835, https://doi.org/10.1039/C9NA00374F.

[52] R. Jayabalan, R.V. Malbaša, E.S. Lončar, J.S. Vitas, M. Sathishkumar, A review on Kombucha tea-microbiology, composition, fermentation, beneficial effects, toxicity, and tea fungus, Compr. Rev. Food Sci. Food Saf. 13 (2014) 538–550, https://doi.org/10.1111/1541-4337.12073.

[53] D. Qu, Z. Sun, The formation mechanism and fluorophores of carbon dots synthesized via a bottom-up route, Mater. Chem. Front. 4 (2020) 400–420, https://doi.org/10.1039/C9QM00552H.

[54] K. Cicek, S. Demirel, Self-healable PVA–graphite–borax as electrode and electrolyte properties for smart and flexible supercapacitor applications, J. Mater. Sci. Mater. Electron. 32 (2021) 16335–16345, https://doi.org/10.1007/s10854-021-06186-w.

[55] H. Quan, W. Zeng, W. Chen, Y. Wang, W. Tao, D. Chen, Carbon quantum dot-induced robust ε-MnO2 electrode by synergistic engineering of oxygen vacancy and low crystallinity for high-performance flexible asymmetric supercapacitor, J. Alloys Compd. 938 (2023), 168524, https://doi.org/10.1016/j.jallcom.2022.168524.

[56] C. Qi, H. Wang, A. Yang, X. Wang, J. Xu, Facile fabrication of highly fluorescent N-doped carbon quantum dots using an ultrasonic-assisted hydrothermal method: optical properties and cell imaging, ACS Omega 6 (2021) 32904–32916, https://doi.org/10.1021/acsomega.1c04903.

[57] T. Yu, H. Wang, C. Guo, Y. Zhai, J. Yang, J. Yuan, A rapid microwave synthesis of green-emissive carbon dots with solid-state fluorescence and pH-sensitive properties, R. Soc. Open Sci. 5 (2018), 180245, https://doi.org/10.1098/rsos.180245.

[58] S.C. Ray, A. Saha, N.R. Jana, R. Sarkar, Fluorescent carbon nanoparticles: synthesis, characterization, and bioimaging application, J. Phys. Chem. C 113 (2009) 18546–18551, https://doi.org/10.1021/jp905912n.

[59] A. Chandra, N. Singh, Biocompatible fluorescent carbon dots for ratiometric intracellular pH sensing, ChemistrySelect 2 (2017) 5723–5728, https://doi.org/10.1002/slct.201701012.

[60] S.-L. Hu, K.-Y. Niu, J. Sun, J. Yang, N.-Q. Zhao, X.-W. Du, One-step synthesis of fluorescent carbon nanoparticles by laser irradiation, J. Mater. Chem. 19 (2009) 484–488, https://doi.org/10.1039/B812943F.

[61] G. Eda, Y.-Y. Lin, C. Mattevi, H. Yamaguchi, H.-A. Chen, I.-S. Chen, C.-W. Chen, M. Chhowalla, Blue photoluminescence from chemically derived graphene oxide, Adv. Mater. 22 (2010) 505–509, https://doi.org/10.1002/adma.200901996.

[62] D. Kong, F. Yan, Y. Luo, Q. Ye, S. Zhou, L. Chen, Amphiphilic carbon dots for sensitive detection, intracellular imaging of Al3+, Anal. Chim. Acta 953 (2017) 63–70, https://doi.org/10.1016/j.aca.2016.11.049.

[63] X. Yang, Y. Zhuo, S. Zhu, Y. Luo, Y. Feng, Y. Dou, Novel and green synthesis of high-fluorescent carbon dots originated from honey for sensing and imaging, Biosens. Bioelectron. 60 (2014) 292–298, https://doi.org/10.1016/j.bios.2014.04.046.

[64] A. Mewada, S. Pandey, S. Shinde, N. Mishra, G. Oza, M. Thakur, M. Sharon, M. Sharon, Green synthesis of biocompatible carbon dots using aqueous extract of Trapa bispinosa peel, Mater. Sci. Eng. C 33 (2013) 2914–2917, https://doi.org/10.1016/j.msec.2013.03.018.

[65] S. Zhao, M. Lan, X. Zhu, H. Xue, T.-W. Ng, X. Meng, C.-S. Lee, P. Wang, W. Zhang, Green synthesis of bifunctional fluorescent carbon dots from garlic for cellular imaging and free radical scavenging, ACS Appl. Mater. Interfaces 7 (2015) 17054–17060, https://doi.org/10.1021/acsami.5b03228.

[66] Y. Fang, S. Guo, D. Li, C. Zhu, W. Ren, S. Dong, E. Wang, Easy synthesis and imaging applications of cross-linked green fluorescent hollow carbon nanoparticles, ACS Nano 6 (2012) 400–409, https://doi.org/10.1021/nn2046373.

[67] C. Zhu, J. Zhai, S. Dong, Bifunctional fluorescent carbon nanodots: green synthesis via soy milk and application as metal-free electrocatalysts for oxygen reduction, Chem. Commun. 48 (2012) 9367, https://doi.org/10.1039/c2cc33844k.

[68] C. Wang, K. Jiang, Z. Xu, H. Lin, C. Zhang, Glutathione modified carbon-dots: from aggregation-induced emission enhancement properties to a “turn-on” sensing of temperature/Fe 3+ ions in cells, Inorg. Chem. Front. 3 (2016) 514–522, https://doi.org/10.1039/C5QI00273G.

[69] P. Das, S. Ganguly, M. Bose, S. Mondal, A.K. Das, S. Banerjee, N.C. Das, A simplistic approach to green future with eco-friendly luminescent carbon dots and their application to fluorescent nano-sensor ‘turn-off’ probe for selective sensing of copper ions, Mater. Sci. Eng. C 75 (2017) 1456–1464, https://doi.org/10.1016/j.msec.2017.03.045.

[70] Y. Fujii, Y. Muramoto, N. Shimizu, Analysis of electric double layer in aqueous solutions of sodium chloride, in: Annu. Rep. - Conf. Electr. Insul. Dielectr. Phenomena, CEIDP, 2010, https://doi.org/10.1109/CEIDP.2010.5724027.

[71] M.J. Carmezim, C.F. Santos, Electrolytes in metal oxide supercapacitors, in: Met. Oxides Supercapacitors, Elsevier, 2017, pp. 49–78, https://doi.org/10.1016/b978-0-12-810464-4.00003-6.